Intrinsic Noise Equivalent-Circuit Parameters for AlGaN/GaN HEMTs

Sungjae Lee, *Student Member, IEEE*, Kevin J. Webb, *Senior Member, IEEE*, Vinayak Tilak, and Lester F. Eastman, *Life Fellow, IEEE*

***Abstract*—Intrinsic noise sources and their correlation in gallium–nitride high electron-mobility transistors are extracted and studied. Microwave noise measurements have been performed over the frequency range of 0.8–5.8 GHz. Using measured noise and scattering parameter data, the gate and drain noise sources and their correlation are determined using an equivalent-circuit representation. This model correctly predicts the frequency-dependent noise for two devices having different gate length. Three noise mechanisms are identified in these devices, namely, those due to velocity fluctuation, gate leakage, and traps.**

***Index Terms*—Correlation, leakage currents, semiconductor device noise, shot noise, white noise.**

I. Introduction

WIDE-BANDGAP aluminum gallium–nitride/gallium–nitride (AlGaN/GaN) high electron-mobility transistors (HEMTs) have recently been studied for high-frequency, high-power, and high-temperature operation due to their high saturated electron drift velocity (1.3×10^7 cm/s), large breakdown field ($E_C > 3$ MV/cm), and good thermal conductivity, particularly with SiC substrates ($\theta \geq 3.3$ W/°K $\cdot$ cm) [1]. Furthermore, the high-speed performance of AlGaN/GaN HEMTs can result in low microwave noise characteristics, making these devices candidates for receivers with a higher breakdown-related receiver damage threshold. For example, minimum microwave noise figures of 0.53 dB at 8 GHz (100-GHz f_T device, $V_{\rm ds} = 8$ V) and 0.4 dB at 5 GHz (58-GHz f_T device, $V_{\rm ds} = 1$ V) have been reported for AlGaN/GaN HEMTs [2], [3]. In the case of transmitter oscillators, low $1/f$ (or flicker) noise is important because the upconversion of $1/f$ noise degrades the system performance. This low-frequency $1/f$-type noise in AlGaN/GaN HEMTs has been associated with contributions from the traps [4]–[6].

Understanding features that impact noise within the intrinsic device, where parasitic and contact contributions to the noise have been deembedded, would provide a path to noise performance interrogation in the still relatively immature GaN HEMTs. Establishing a noise equivalent-circuit model permits extraction of the intrinsic noise properties of AlGaN/GaN HEMTs, allowing performance prediction and study of noise mechanisms within the device. For example, this model could allow the prediction of oscillator phase noise, receiver noise, and the influence of physical effects such as traps and contacts. Furthermore, having a good noise model allows for circuit design.

Noise models can be broadly classified into numerical and experimental approaches, both of which could lead to an equivalent-circuit representation with adequate parameterization. While Monte Carlo numerical studies can lead to port noise [7], the more tractable Green's function approach based on the trans-impedance concept of Shockley *et al.* [8] has been commonly applied [9]. The experimental two-port characterization yields three noise parameters, i.e., the minimum noise figure ($F_{\rm min}$), noise resistance (R_n or conductance G_n), and optimum source admittance for minimum noise ($Y_{\rm opt} = G_{\rm opt} + jB_{\rm opt}$) [10]. With scattering (S)-parameter measurements, these measured noise parameters can be coupled to an equivalent-circuit model, an approach that is common for microwave devices. An empirical relation between the noise figure and circuit parameters employing fitting parameters was proposed for GaAs FETs by Fukui [11]. More quantitative equivalent-circuit modeling has been pursued by Statz *et al.* [12] and Pospieszalski [13], where the noise was represented equivalently as gate and drain temperature or resistance/conductance using Nyquist noise sources. In the case of the fundamental noise due to velocity fluctuations of the electrons in the channel, one would anticipate correlation between these gate and drain noise sources. The extraction of this correlation, necessary for the complete frequency-dependent model, has received little attention. It has, however, been predicted numerically [9]. While the correlation was incorporated into the convenient extraction model proposed by Pucel *et al.* [14], it was not specifically studied. In other experimental work where the correlation was specifically addressed, it has not been treated rigorously as a free variable [13], [15], [16]. Thus far, noise equivalent-circuit models for GaN HEMTs have received little attention [3], [17], [18].

We report here the extraction of the intrinsic noise sources and their correlation in AlGaN/GaN HEMTs. Furthermore, the two-port model presented can be generalized to any two-port system. Using microwave noise and S-parameter measurement results, the intrinsic noise sources are extracted by means of a deembedding routine suggested by Pucel *et al.* [14] with a modified noise model. The intrinsic gate and drain noise currents and their correlation are presented as a function of

Manuscript received August 19, 2002. This work was supported in part by the Office of Naval Research under Contract N00014-98-1-0371, Contract N00014-99-C-0172, and Contract N00014-98-1-0371.

S. Lee and K. J. Webb are with the School of Electrical and Computer Engineering, Purdue University, West Lafayette, IN 47907 USA (e-mail: webb@ecn.purdue.edu).

V. Tilak was with the School of Electrical Engineering, Cornell University, Ithaca, NY 14853 USA. He is now with Central Research and Development Laboratories, General Electric, Niskayuna, NY 12304 USA.

L. F. Eastman is with the School of Electrical Engineering, Cornell University, Ithaca, NY 14853 USA.

Digital Object Identifier 10.1109/TMTT.2003.810140

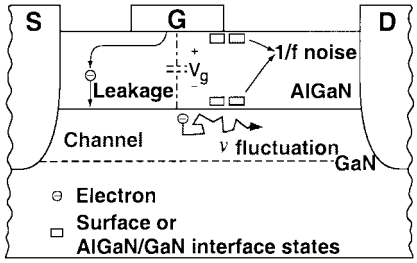

Fig. 1. Fundamental noise mechanisms in AlGaN/GaN HEMTs.

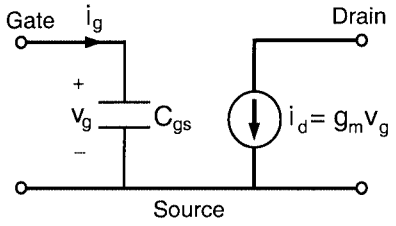

Fig. 2. Ideal FET model with white noise random variables i_d and v_g.

drain-to-source voltage $(V_{\rm ds})$, current $(I_{\rm ds})$, and operating frequency (0.8–5.8 GHz). The noise equivalent-circuit model is enhanced to accommodate the independent velocity fluctuation, gate leakage shot noise, and $1/f$ noise we have observed. Using this model, the intrinsic noise sources and their values, deembedded at one frequency, are used to simulate the noise parameters (e.g., the minimum noise figure $F_{\rm min}$) at other frequencies. This assumes that the frequency dependence of the $1/f$ noise for the AlGaN/GaN HEMTs is known and deembedded correctly from the total noise, and that the other microwave noise sources (velocity fluctuation and gate leakage shot noise) in the frequency range of interest are frequency independent.

II. Theory

A. Noise Mechanisms in AlGaN/GaN HEMTs

We assume that there are three uncorrelated noise mechanisms in the intrinsic HEMT, associated with velocity fluctuation, gate leakage, and traps, as shown in the schematic of Fig. 1. The velocity fluctuation or diffusion noise is due to electron scatter from the heterojunction, the lattice (phonon), and impurities. This diffusion noise contracts to thermal or Johnson noise if the Einstein relation holds [19]. The bandwidth of this process is proportional to the inverse of the scattering time, making it frequency independent (i.e., white noise) in the microwave regime where we have performed measurements. This fundamental noise process results in a drain current noise variance $(\langle|i_d|^2\rangle)$ that will be ideally white and dominated by the channel conduction process. The associated gate voltage variance $(\langle|v_g|^2\rangle)$ is coupled to the channel random process by the gate capacitance $(C_{\rm gs})$. Physically, one could view this as a random variation in the electric-field lines that terminate on the local random variation in channel charge, due to velocity fluctuation, and the induced gate charge. The line integral of this field gives the gate voltage. A frequency-independent $\langle|i_d|^2\rangle$ will, therefore, result in $\langle|v_g|^2\rangle$ being frequency independent. This model suggests that the correlation between the gate (v_g) and drain (i_d) noise sources will be a function of the degree of electron scatter in the channel, and that it would tend to reduce with increasing channel length. The gate leakage noise process is associated with electron injection into the channel over the gate Schottky barrier. The randomness of this emission process would lead to classical shot noise ($\langle|i|^2\rangle = 2eI_g$ A^2/Hz, with $e = 1.6 \times 10^{-19}$ C and I_g the gate dc current) [19]. This gate leakage noise is also ideally independent of frequency. Finally, we assume a $1/f^{\alpha}$ noise process due to the trapping of electrons in surface states (near the gate) or AlGaN/GaN interface states (near the channel). All three of these noise processes will contribute to both the gate and drain noise variances. In addition to the intrinsic noise sources, there is thermal noise associated with various resistances, including source and drain contact resistance and gate finger resistance. All of these noise sources are uncorrelated with each other and with the intrinsic noise. The purpose of this paper is to deembed the parasitic contribution from the total noise and to study the intrinsic noise sources within the device.

B. Ideal FET Noise

Consider the simple FET circuit model of Fig. 2 with a white noise process in the channel that results in i_d and v_g being frequency independent and perfectly correlated. The random drain current is $i_d = g_m v_g$, where g_m is the transconductance, and $i_g = j2\pi f C_{\rm gs} v_g$, with $C_{\rm gs}$ being the gate-to-source capacitance. Thus, with perfect correlation assumed in this ideal noise model

$$\langle i_g i_d^* \rangle = j2\pi f C_{\rm gs} g_m \langle |v_g|^2 \rangle \tag{1}$$

$$\langle |i_g|^2 \rangle = 4\pi^2 f^2 C_{\rm gs}^2 \langle |v_g|^2 \rangle \tag{2}$$

$$\langle |i_d|^2 \rangle = g_m^2 \langle |v_g|^2 \rangle. \tag{3}$$

If i_d is frequency independent, then this model results in v_g being independent of frequency, $\langle|i_g|^2\rangle \propto f^2$ and $\langle i_g i_d^* \rangle \propto jf$.

C. Two-Port Noise Figure

As suggested by Rothe and Dahlke [10], all noise within a two-port device can be represented as two equivalent and partially correlated noise sources (a random voltage v_A and a random current i_A) at the input of the same two-port device, now considered noiseless, as shown in Fig. 3(a). Writing

$$i_A = Y_c v_A + i_u \tag{4}$$

where v_A and i_u are uncorrelated and Y_c $(=G_c + jB_c)$ is a correlation admittance, two independent noise sources (v_A, i_u) can be used, as in Fig. 4. This allows the convenient expression of the two-port noise figure and other noise parameters using superposition.

We assume a zero mean Gaussian noise model. The variance of the noise sources in Fig. 4 can be written using Nyquist's theorem [20] as

$$\langle |v_A|^2 \rangle = 4kT_0 B R_n \tag{5}$$

$$\langle |i_u|^2 \rangle = 4kT_0 B G_n \tag{6}$$

where $\langle\ \rangle$ denotes the statistical average, k is the Boltzmann's constant, T_0 is room temperature (290 K), B is the noise bandwidth (1 Hz throughout this paper), and the values of R_n and

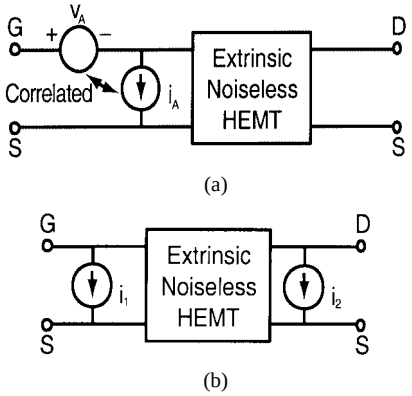

Fig. 3. (a) Equivalent noise circuit with noise sources (v_A and i_A) at the input ($ABCD$ representation). (b) Equivalent noise circuit with current noise sources (i_1, i_2) at the input and output (Y representation).

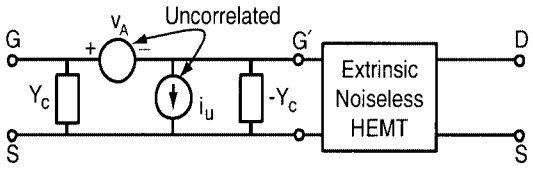

Fig. 4. Equivalent noise circuit with two independent noise sources and a correlation admittance ($i_A = Y_c v_A + i_u$).

G_n determine the variances. The two-port noise figure F ($=1+\langle|i|^2\rangle_{G'}/\langle|i|^2\rangle_G$) in Fig. 4) is defined as the ratio of the input to output signal-to-noise ratio, which for Fig. 4 with source admittance Y_s ($=G_s + jB_s$) becomes [10]

$$F = 1 + \frac{1}{G_s}\left[G_n + R_n|Y_s + Y_c|^2\right]. \tag{7}$$

Partial derivatives of (7) with respect to G_s and B_s ($\partial F/\partial G_s = 0, \partial F/\partial B_s = 0$) give the optimum value of Y_s for the minimum F. This optimum input admittance $Y_{\rm opt}$ ($=G_{\rm opt} + jB_{\rm opt}$) is given by

$$Y_{\rm opt} = \sqrt{\frac{G_n}{R_n} + G_c^2} + j(-B_c). \tag{8}$$

Substituting $Y_s = Y_{\rm opt}$ into (7) gives

$$F_{\rm min} = 1 + 2R_nG_c + 2R_n\sqrt{\frac{G_n}{R_n} + G_c^2}. \tag{9}$$

Rather than expressing F as a function of G_n and Y_c, as in (7), it can be expressed in terms of $F_{\rm min}$ and $Y_{\rm opt}$ as

$$F = F_{\rm min} + \frac{R_n}{G_s}|Y_s - Y_{\rm opt}|^2. \tag{10}$$

Measurement of the noise figure for various Y_s allows the determination of $F_{\rm min}$, R_n, and $Y_{\rm opt}$ in (10) by means of a least mean square error fit to $F(Y_s)$ [21]. The parameters G_c, B_c, and G_n can then be evaluated from (8) and (9). Measurements of this type are common, and research has been done, for example, to relate the data to noise sources within GaAs and CMOS devices [15], [22].

D. Noise Correlation Matrix

In addition to the $ABCD$ (or chain) representation of Fig. 3(a), the admittance (or Y) topology, displayed in Fig. 3(b), can model any linear noisy two-port. In each case, the noise sources can be correlated. The self- and cross-power spectral densities of the two-port noise sources in $ABCD$ matrix form are [23]

$$\mathbf{C}_A = \begin{bmatrix} \langle v_A v_A^* \rangle & \langle v_A i_A^* \rangle \\ \langle i_A v_A^* \rangle & \langle i_A i_A^* \rangle \end{bmatrix} \tag{11}$$

where v_A and i_A are the two noise sources at the input of the noiseless two port system in Fig. 3(a). Similarly, the noise correlation matrix using the admittance form of Fig. 3(b) is

$$\mathbf{C}_Y = \begin{bmatrix} \langle i_1 i_1^* \rangle & \langle i_1 i_2^* \rangle \\ \langle i_2 i_1^* \rangle & \langle i_2 i_2^* \rangle \end{bmatrix}. \tag{12}$$

As one can determine the two-port $ABCD$-parameters by knowing either Y- or Z-parameters (or vice versa) using their defining relations, the conversion can also be made between any two representations of a linear noisy two-port. Likewise, transformation from one type of noise correlation matrix to the other (e.g., from $\mathbf{C}_A$ to $\mathbf{C}_Y$) can be achieved.

While $\mathbf{C}_Y$ is convenient for transistor models with equivalent gate and drain noise sources, $\mathbf{C}_A$ is easier to obtain from the noise measurement because there is a direct relation between the measured noise parameters ($F_{\rm min}$, R_n, and $Y_{\rm opt}$) and the noise sources at the input of the noiseless two-port (v_A, i_A), i.e., R_n, G_n, and Y_c [see (8) and (9)]. As shown in the Appendix, $\mathbf{C}_A$ can be expressed in terms of $F_{\rm min}$, R_n, and $Y_{\rm opt}$ as

$$\mathbf{C}_A = \begin{bmatrix} R_n & \dfrac{F_{\rm min}-1}{2} - R_nY_{\rm opt}^* \\ \dfrac{F_{\rm min}-1}{2} - R_nY_{\rm opt} & R_n|Y_{\rm opt}|^2 \end{bmatrix} \tag{13}$$

where the elements have been normalized by $4kT_0B$, a practice that continues henceforth.

III. Noise Source Deembedding

A. Linear Noisy Two-Port Equivalent Circuit

Fig. 5 shows the noiseless intrinsic transistor small-signal equivalent circuit with partially correlated gate noise (i_g) and drain noise (i_d) currents. The circuit parameters inside the dashed box (as well as the parasitics in Fig. 6) can be obtained from S-parameter measurements. Compared with the ideal input circuit of Fig. 2, $R_{\rm gs}$ is the resistance responsible for the gate leakage current and R_i is the channel resistance. The value of $R_{\rm gs}$ is large relative to $|1/j2\pi fC_{\rm gs}|$, allowing $R_{\rm gs}$ to be excluded from the equivalent circuit of Fig. 5 when the element values are determined based on microwave S-parameter measurements. While R_i is retained during parameter extraction, for the measurement frequency range, $|1/j2\pi fC_{\rm gs}| \gg R_i$. The ideal noise model of Fig. 2 thus becomes a reasonable approximation.

Fig. 6 shows the parasitic gate finger resistance R_g, the source contact resistance R_s, and the drain contact resistance R_d, and their noise contribution or equivalent noise current sources (i_{p1}, i_{p2}, i_{p3}, i_{p4}). The noiseless extrinsic transistor, including parasitic elements, and its equivalent noise sources (i_{n1}, i_{n2}), are given in Fig. 7. In Fig. 7, $\mathbf{Y}_d$ is the small-signal admittance matrix for the intrinsic transistor (representing the circuit inside the dashed box in Fig. 5). Note that the intrinsic noise sources (i_g, i_d) in Fig. 5, and the parasitic noise sources (i_{p1}, i_{p2}, i_{p3}, i_{p4}) in Fig. 6, are absorbed into i_{n1} and i_{n2}, the only noise sources

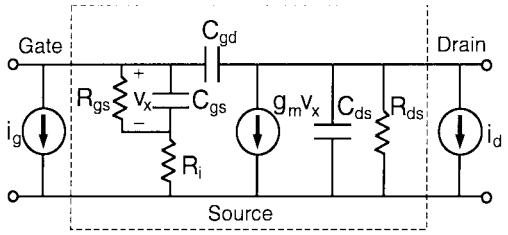

Fig. 5. Intrinsic noise equivalent-circuit model (admittance form) with i_g and i_d representing partially correlated intrinsic noise sources. Inside the dashed box is now a noiseless two-port intrinsic transistor, and v_x is the deterministic drive signal.

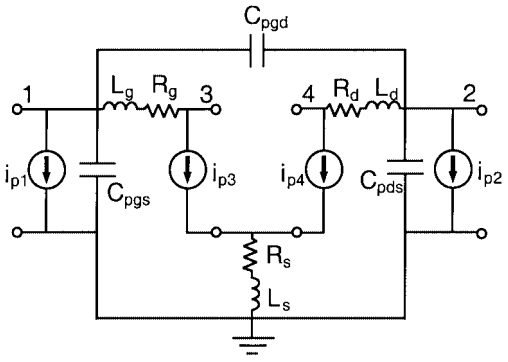

Fig. 6. Parasitic four-port network with its equivalent noise currents (i_{p1}, i_{p2}, i_{p3}, i_{p4}) in admittance form.

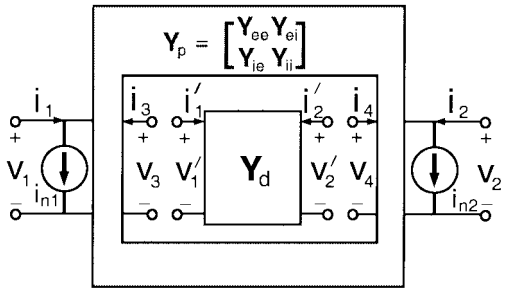

Fig. 7. Noiseless extrinsic transistor (within the shaded box) and its additional noise sources (i_{n1}, i_{n2}) in admittance form. The intrinsic transistor in Fig. 5 is represented by $\mathbf{Y}_d$ and the external parasitics are represented by $\mathbf{Y}_p$, which is partitioned into four 2×2 submatrices $\mathbf{Y}_{ee}$, $\mathbf{Y}_{ei}$, $\mathbf{Y}_{ie}$, and $\mathbf{Y}_{ii}$.

in Fig. 7. The 4×4 parasitic admittance matrix $\mathbf{Y}_p$ is partitioned into four 2×2 submatrices, $\mathbf{Y}_{ee}$, $\mathbf{Y}_{ei}$, $\mathbf{Y}_{ie}$, and $\mathbf{Y}_{ii}$, as in Fig. 7. Thus, the port currents in Fig. 6 become

$$\begin{bmatrix} i_1 \\ i_2 \end{bmatrix} = \mathbf{Y}_{ee} \begin{bmatrix} v_1 \\ v_2 \end{bmatrix} + \mathbf{Y}_{ei} \begin{bmatrix} v_3 \\ v_4 \end{bmatrix} + \begin{bmatrix} i_{p1} \\ i_{p2} \end{bmatrix} \tag{14}$$

$$\begin{bmatrix} i_3 \\ i_4 \end{bmatrix} = \mathbf{Y}_{ie} \begin{bmatrix} v_1 \\ v_2 \end{bmatrix} + \mathbf{Y}_{ii} \begin{bmatrix} v_3 \\ v_4 \end{bmatrix} + \begin{bmatrix} i_{p3} \\ i_{p4} \end{bmatrix}. \tag{15}$$

The defining relation between (v_1', v_2') and (i_1', i_2') in Fig. 7, using the noise sources in the equivalent circuit of Fig. 5, is

$$\begin{bmatrix} i_1' \\ i_2' \end{bmatrix} = \mathbf{Y}_d \begin{bmatrix} v_1' \\ v_2' \end{bmatrix} + \begin{bmatrix} i_g \\ i_d \end{bmatrix}. \tag{16}$$

Applying the boundary conditions ($v_3 = v_1'$, $v_4 = v_2'$, $i_3 = -i_1'$, and $i_4 = -i_2'$ in Fig. 7) to (15) and (16) to solve for the relationship between (v_1, v_2) and (v_3, v_4), and using that relationship in (14), the extrinsic port currents can be expressed as

$$\begin{bmatrix} i_1 \\ i_2 \end{bmatrix} = \mathbf{Y}_e \begin{bmatrix} v_1 \\ v_2 \end{bmatrix} + \begin{bmatrix} i_{p1} \\ i_{p2} \end{bmatrix} + \mathbf{W} \begin{bmatrix} i_{p3} \\ i_{p4} \end{bmatrix} + \mathbf{W} \begin{bmatrix} i_g \\ i_d \end{bmatrix} \tag{17}$$

where $\mathbf{Y}_e$ represents the two-port network for the extrinsic (intrinsic + parasitic) noiseless transistor, derived as

$$\mathbf{Y}_e = \mathbf{Y}_{ee} + \mathbf{W}\mathbf{Y}_{ie} \tag{18}$$

and

$$\mathbf{W} = -\mathbf{Y}_{ei}(\mathbf{Y}_{ii} + \mathbf{Y}_d)^{-1}. \tag{19}$$

Equation (17) indicates that the equivalent extrinsic noise sources (i_{n1}, i_{n2}) of Fig. 7 can be expressed as a linear superposition of the intrinsic and parasitic noise sources of Figs. 5 and 6, respectively. From (17), setting $\mathbf{i}_{\text{ex}} = [i_{n1}\ i_{n2}]^T$, $\mathbf{i}_p = [i_{p1}\ i_{p2}\ i_{p3}\ i_{p4}]^T$ [from (14) and (15)], and $\mathbf{i}_{\text{in}} = [i_g\ i_d]^T$ [from (16)], where T denotes the transpose

$$\mathbf{i}_{\text{ex}} = \mathbf{P}\mathbf{i}_p + \mathbf{W}\mathbf{i}_{\text{in}} \tag{20}$$

where the 2×4 matrix $\mathbf{P} = [\mathbf{U}|\mathbf{W}]$, with $[\mathbf{U}]$ being the 2×2 identity matrix.

The noise correlation matrices for the intrinsic device and the parasitics, defined in the admittance form of (12) as $\langle \mathbf{i}_{\text{in}} \mathbf{i}_{\text{in}}^H \rangle$ and $\langle \mathbf{i}_p \mathbf{i}_p^H \rangle$, respectively, where H denotes Hermitian (complex conjugate transpose), are

$$\mathbf{C}_d = \begin{bmatrix} \langle i_g i_g^* \rangle & \langle i_g i_d^* \rangle \\ \langle i_d i_g^* \rangle & \langle i_d i_d^* \rangle \end{bmatrix} \tag{21}$$

$$\mathbf{C}_p = \begin{bmatrix} \mathbf{C}_{ee} & \mathbf{C}_{ei} \\ \mathbf{C}_{ie} & \mathbf{C}_{ii} \end{bmatrix} \tag{22}$$

where $\mathbf{C}_{ee}$, $\mathbf{C}_{ei}$, $\mathbf{C}_{ie}$, and $\mathbf{C}_{ii}$ are 2×2 submatrices with the same format as used for $\mathbf{Y}_p$. For example,

$$\mathbf{C}_{ei} = \begin{bmatrix} \langle i_{p1} i_{p3}^* \rangle & \langle i_{p1} i_{p4}^* \rangle \\ \langle i_{p2} i_{p3}^* \rangle & \langle i_{p2} i_{p4}^* \rangle \end{bmatrix}.$$

Applying (20) to the noise correlation matrix for the extrinsic device $\mathbf{C}_{pd}$, defined as $\langle \mathbf{i}_{\text{ex}} \mathbf{i}_{\text{ex}}^H \rangle$

$$\mathbf{C}_{pd} = \left\langle (\mathbf{P}\mathbf{i}_p + \mathbf{W}\mathbf{i}_{\text{in}})(\mathbf{P}\mathbf{i}_p + \mathbf{W}\mathbf{i}_{\text{in}})^H \right\rangle. \tag{23}$$

The noise from the parasitic (passive) elements is thermal and uncorrelated with the intrinsic noise sources. Therefore, using this zero correlation between $\mathbf{i}_p$ and $\mathbf{i}_{\text{in}}$, and the definitions for $\mathbf{C}_d$ and $\mathbf{C}_p$ in (21) and (22), $\mathbf{C}_{pd}$ in (23) becomes

$$\mathbf{C}_{pd} = \mathbf{P}\mathbf{C}_p\mathbf{P}^H + \mathbf{W}\mathbf{C}_d\mathbf{W}^H. \tag{24}$$

Reducing (24) to an equation with only 2×2 matrices by using $\mathbf{P} = [\mathbf{U}|\mathbf{W}]$ and (22)

$$\mathbf{C}_{pd} = \mathbf{C}_{ee} + \mathbf{W}\mathbf{C}_{ie} + \mathbf{C}_{ei}\mathbf{W}^H + \mathbf{W}(\mathbf{C}_{ii} + \mathbf{C}_d)\mathbf{W}^H. \tag{25}$$

B. Intrinsic Noise-Source Extraction

The deembedding routine to extract the intrinsic noise sources (i_g and i_d) and their correlation for the AlGaN/GaN HEMT starts from $\mathbf{C}_A$ (11), obtained from the measured noise parameters ($F_{\min}$, R_n, and Y_{opt}) using (13). $\mathbf{C}_A$ is then transformed to its equivalent admittance form $\mathbf{C}_{pd}$ by [23]

$$\mathbf{C}_{pd} = \mathbf{V}\mathbf{C}_A\mathbf{V}^H \tag{26}$$

where $\mathbf{V}$ is the transformation matrix from $\mathbf{C}_A$ to $\mathbf{C}_Y$ given by

$$\mathbf{V} = \begin{bmatrix} -y_{e,11} & 1 \\ -y_{e,21} & 0 \end{bmatrix} \tag{27}$$

with $y_{e,11}$ and $y_{e,21}$ being the $(1,1)$ and $(2,1)$ elements of $\mathbf{Y}_e$, respectively, the 2×2 matrix defined in (18). The noise contribution from the parasitic elements $(\mathbf{C}_p)$ is then stripped from the extrinsic transistor noise $(\mathbf{C}_{pd})$, yielding $\mathbf{C}_d$, the normalized noise spectral power of the intrinsic transistor. In order to obtain $\mathbf{C}_p$, we use a generalization of Nyquist's theorem for linear passive networks due to Twiss, who showed that $\langle i_m i_n^* \rangle = (1/2)(y_{mn} + y_{nm}^*)$ in normalized form, where $i_{m,n}$ is the short-circuit noise current at the (m, n)th port and y_{mn} is the associated element of the network admittance matrix [24]. Therefore, the noise correlation matrix of the four-port parasitic network in Fig. 6, i.e., $\mathbf{C}_p$, can be represented by

$$\mathbf{C}_p = \frac{1}{2}\left(\mathbf{Y}_p + \mathbf{Y}_p^H\right) \tag{28}$$

where the elements of $\mathbf{Y}_p$, given in Fig. 7, can be obtained from the modeled device parasitics. Finally, by inverting (25), the resulting noise correlation matrix for the intrinsic transistor $\mathbf{C}_d$ is

$$\mathbf{C}_d = \mathbf{W}^{-1}(\mathbf{C}_{pd} - \mathbf{C}_{ee})\left(\mathbf{W}^{-1}\right)^H - \mathbf{C}_{ie}\left(\mathbf{W}^{-1}\right)^H - \mathbf{W}^{-1}\mathbf{C}_{ei} - \mathbf{C}_{ii} \tag{29}$$

where $\mathbf{C}_{ee}$, $\mathbf{C}_{ei}$, $\mathbf{C}_{ie}$, $\mathbf{C}_{ii}$ can be determined using (28).

The elements of $\mathbf{C}_d$ are represented by i_g, i_d, and their correlation. The correlation coefficient C is defined in normalized form as [12]

$$C = \frac{\langle i_g i_d^* \rangle}{\sqrt{\langle |i_g|^2 \rangle \langle |i_d|^2 \rangle}}. \tag{30}$$

With perfect correlation assumed in the ideal noise model of Fig. 2, and using (1)–(3) in (30), $C = j1$.

The noise extraction steps described in this section were implemented using MATLAB. The measured S-parameter data was used in Agilent EEsof Advanced Design System (ADS) software to determine the extrinsic (intrinsic and parasitic) equivalent-circuit parameters for the model in Figs. 5 and 6. These equivalent-circuit parameters were transformed to admittance matrices $\mathbf{Y}_d$ and $\mathbf{Y}_p$ using MATLAB. These admittance parameters, together with the measured noise parameters $(F_{\min}, R_n, Y_{\text{opt}})$ were used as input parameters in (13), (18), (19), and (28) to determine the intrinsic noise correlation matrix $\mathbf{C}_d$ using (26), (27), and (29).

IV. Microwave Noise and S-Parameter Measurement

The noise properties of AlGaN/GaN HEMTs on SiC substrates, originally designed and fabricated for high-power density operation [1], were investigated. These devices had a 200-Å AlN nucleation layer, a 3-μm undoped GaN buffer layer, a 200-Å $Al_{0.3}Ga_{0.7}N$ layer, and a 20-Å GaN cap layer. The devices were passivated with an Si_3N_4 layer. Previous studies have indicated that this passivation suppresses the surface states that limit the large-signal microwave characteristics [25]. Fig. 8 shows the dc I–V characteristics of a 0.25 $\times$ 250 μm^2 AlGaN/GaN HEMT device.

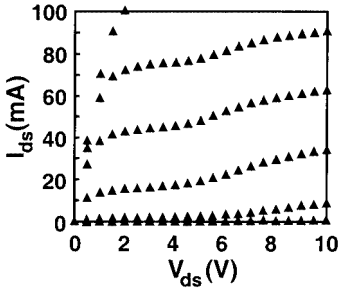

Fig. 8. DC I–V characteristics of 0.25 $\times$ 250 μm^2 AlGaN/GaN HEMT. $V_{\text{gs}} = -3.0$ V to -5.5 V with a step size of -0.5 V. The microwave noise figure was measured for $V_{\text{ds}} = 0.5, 1, 2, 4, 6, 8, 10$ V, and for each voltage, $I_{\text{ds}} = 10$ to 100 mA, with a step size of 10 mA.

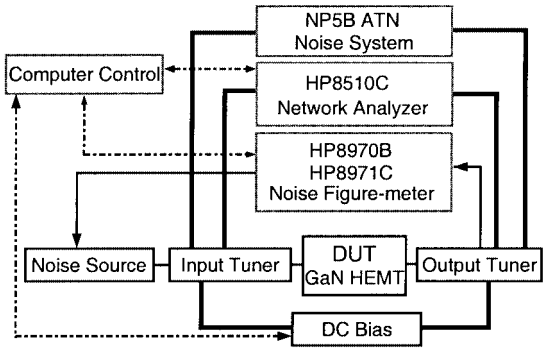

Fig. 9. ATN NP5B load–pull noise measurement setup. The F is measured with varying Y_s, achieved with the input tuner, and the fundamental noise parameters are extracted by built-in software.

The set of S-parameter data was obtained using an HP8510B vector network analyzer, and the measured data was used to determine extrinsic (intrinsic + parasitic) device parameters. The small-signal intrinsic and extrinsic device parameters (i.e., $\mathbf{Y}_d$ and $\mathbf{Y}_p$) were used in the extraction of intrinsic noise sources. On-wafer microwave noise measurements were performed using an ATN NP5B system, shown schematically in Fig. 9 [26]. The input tuner provides multiple source terminations (16 different Y_s were provided in the measurement), and the basic noise parameters $F_{\min}$, R_n, and Y_{opt} were extracted as a function of frequency and bias by built-in software using this load–pull data. The frequency range (0.8–5.8 GHz) of the noise measurement was dictated by the electric tuners used. The repeatability of the calibration and measurement was estimated by two sets of calibration and measurement data for the same 0.25 $\times$ 250 μm^2 AlGaN/GaN HEMT. The difference between the measured $F_{\min}$ in the frequency of 0.8–5.8 GHz was within 0.1 dB. Also, after each calibration, $F_{\min}$ of a standard 6-dB pad was measured in order to verify the accuracy of the calibration.

Fig. 10 shows the noise measurement results for 0.25 $\times$ 250 μm^2 and 0.4 $\times$ 250 μm^2 AlGaN/GaN HEMTs on SiC substrates. The $F_{\min}$ and associated gain versus frequency (0.8–5.8 GHz) are displayed, where the associated gain is the available gain of the device when $Y_s = Y_{\text{opt}}$. Fig. 10 indicates that the longer gate-length device has higher noise figure and lower gain. This is consistent with noise performance scaling with the transit frequency f_T $(=g_m/2\pi C_{\text{gs}})$, i.e., that higher device speed (smaller C_{gs}) results in lower noise. For our

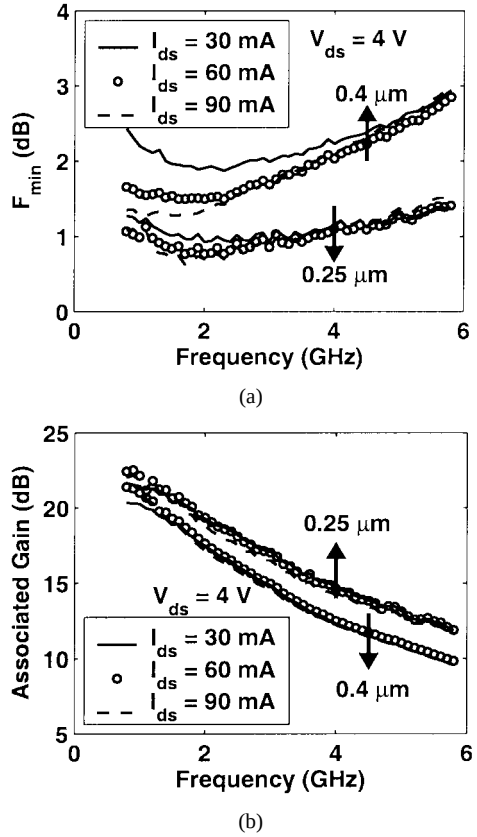

Fig. 10. (a) $F_{\min}$ for the 0.25 × 250 μm^2 and 0.4 × 250 μm^2 AlGaN/GaN HEMTs at $V_{\rm ds} = 4$ V and $I_{\rm ds} = 30, 60, 90$ mA. (b) Associated gain.

250-μm gate periphery AlGaN/GaN power HEMT devices, a minimum noise figure of 1.27 dB (13.21-dB associated gain) at 5 GHz ($V_{\rm ds} = 4$ V, $I_{\rm ds} = 60$ mA) and 0.75 dB (17.5-dB associated gain) at 2 GHz ($V_{\rm ds} = 2$ V, $I_{\rm ds} = 30$ mA) were measured.

V. Intrinsic Noise Extraction From Experimental Data

The intrinsic noise properties were obtained by applying the deembedding routine described in Section III to the measured S-parameter and noise data for the 0.25 × 250 μm^2 and 0.40 × 250 μm^2 AlGaN/GaN HEMTs. We describe some specific steps to achieve the intrinsic device model and then present the noise data.

The parasitic capacitances (C_{pgs}, C_{pds}, and C_{pgd}) in Fig. 6 can be determined from S-parameters measured with $V_{\rm gs}$ set below the pinchoff voltage and $V_{\rm ds} = 0$ V, where the only remaining extrinsic elements are the pad capacitances in a π configuration. Their values can be determined using the Y-parameters obtained from the measured S-parameters, a step taken in a prior study [27]. The parasitic resistances and inductances in Fig. 6 were obtained using S-parameter measurements with the gate-to-source junction forward biased, and with $V_{\rm ds}$ set to zero. The equivalent circuit in Fig. 6 contains the parasitic resistances (R_g, R_s, R_d) and inductances (L_g, L_s, L_d) along with the already determined parasitic capacitances. These elements were found from the Z-parameters, determined from the S-parameter data. The two port Y-parameters for the intrinsic device of

TABLE I
Intrinsic and Extrinsic Device Circuit Parameters in Figs. 5 and 6 for the 0.25 × 250 μm^2 AlGaN/GaN HEMT Extracted at $V_{\rm ds} = 4$ V and $I_{\rm ds} = 60$ mA. Note That the Time Delay Associated With g_m was Assumed to be Zero and That $R_{\rm gs}$, Responsible for the Leakage Current, was Large and, Thus, Excluded

C_{gs}	C_{gd}	C_{ds}	R_i	g_m	R_{ds}	R_{gs}	R_g
0.29 pF	0.042 pF	0.033 pF	5.67 Ω	73.78 mS	249.45 Ω	∞	6.68 Ω
C_{pgs}	C_{pgd}	C_{pds}	R_s	R_d	L_g	L_s	L_d
0.003 pF	0.004 pF	0.005 pF	3.6 Ω	4 Ω	39 pH	0 pH	80.4 pH

Fig. 5 were found at each bias point by similar two-port parameter manipulations, from which the equivalent-circuit element values were determined. Table I lists the extracted parameters for the 0.25 × 250 μm^2 AlGaN/GaN HEMT at $V_{\rm ds} = 4$ V and $I_{\rm ds} = 60$ mA.

We first consider the 0.25-μm gate-length device. Fig. 11 shows the intrinsic noise variances $\langle|i_g|^2\rangle$, $\langle|i_d|^2\rangle$ and the correlation coefficient C (magnitude and phase) versus frequency (0.8–5.8 GHz). For $\langle|i_g|^2\rangle$ and $|\langle i_g i_d^*\rangle|$, $I_{\rm ds} = 60$ mA. For $\langle|i_d|^2\rangle$, $I_{\rm ds} = 30, 60, 90$ mA, and at each current, $V_{\rm ds} = 6, 8, 10$ V. Note that $\langle|i_g|^2\rangle$, $\langle i_g i_d^*\rangle$, and $\langle|i_d|^2\rangle$ are plotted on logarithmic magnitude and frequency scales to more clearly show the frequency dependence of the noise. At higher frequencies, $\langle|i_d|^2\rangle$ is practically independent of frequency, $\langle|i_g|^2\rangle$ has f^2 dependence (slope 2), and $|\langle i_g i_d^*\rangle|$ increases linearly with frequency (slope 1). Fig. 11(d) shows that the phase of C is close to 90° at higher frequencies. These frequency dependences of the extracted noise sources are well explained by the ideal velocity fluctuation noise model in Fig. 2 [see also (1)–(3)] [28]. However, the extracted $\langle|i_d|^2\rangle$ and $\langle|i_g|^2\rangle$ increase at lower frequencies, as does the measured $F_{\min}$ in Fig. 10(a). Using the same calibration set and measurement system, $F_{\min}$ of a GaAs pseudomorphic high electron-mobility transistor (pHEMT) was also measured. This GaAs pHEMT data did not show an increase in $F_{\min}$ at lower frequencies. The data for the GaN HEMT suggests that a $1/f$-type noise may be contributing significantly below 2.5 GHz. Furthermore, the $|C|$ reduces at the lower frequencies, suggesting an uncorrelated process. Also, note that the $\langle|i_d|^2\rangle$ increases with $I_{\rm ds}$ in Fig. 11(b), an indication of a shot-type channel noise process.

Our observation of AlGaN/GaN HEMT noise suggests a modified noise model to accommodate three independent (uncorrelated) noise processes. Therefore, we write

$$\langle|i_g|^2\rangle = \langle|i_{g,v}|^2\rangle + \langle|i_{g,\rm shot}|^2\rangle + \langle|i_{g,1/f}|^2\rangle \quad (31)$$

$$\langle|i_d|^2\rangle = \langle|i_{d,v}|^2\rangle + \langle|i_{d,\rm shot}|^2\rangle + \langle|i_{d,1/f}|^2\rangle \quad (32)$$

$$\langle i_g i_d^*\rangle = \langle i_{g,v} i_{d,v}^*\rangle + \langle i_{g,\rm shot} i_{d,\rm shot}^*\rangle + \langle i_{g,1/f} i_{d,1/f}^*\rangle \quad (33)$$

where the subscripts v, shot, and $1/f$ denote velocity fluctuation, shot, and $1/f$ noise, respectively. Note that the injected electrons from the Schottky gate to the channel (as shown in Fig. 1) not only flow into the source (by negative $V_{\rm gs}$), but also flow into the drain when $V_{\rm ds}$ is applied, thus inducing the $i_{d,\rm shot}$ as well as $i_{g,\rm shot}$ [29]. Therefore, we assume that $i_{g,\rm shot}$ and $i_{d,\rm shot}$ have a 180° phase difference. Shown in Fig. 12 for reference are the extracted $\langle|i_g|^2\rangle$, $|\langle i_g i_d^*\rangle|$, and $\langle|i_d|^2\rangle$ for $V_{\rm ds} = 4$

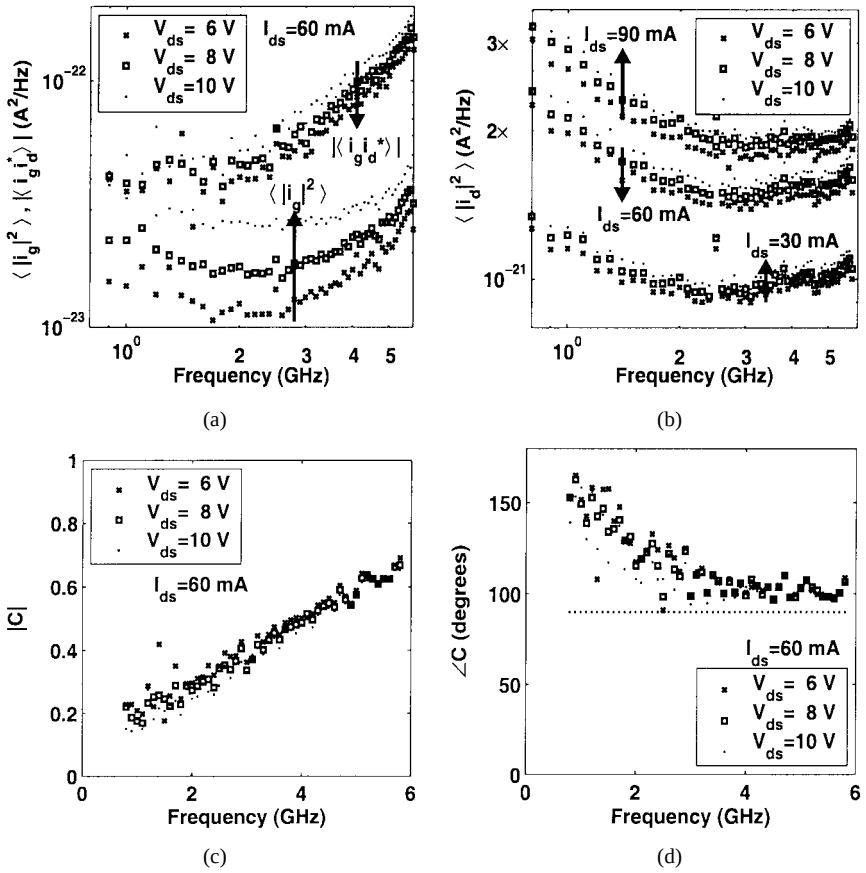

Fig. 11. (a) Intrinsic gate noise variance $\langle |i_g|^2 \rangle$ and correlated spectral density magnitude $|\langle i_g i_d^* \rangle|$ as a function of frequency for $V_{\rm ds} = 6, 8, 10$ V, with $I_{\rm ds} = 60$ mA. (b) $\langle |i_d|^2 \rangle$ for $I_{\rm ds} = 30, 60, 90$ mA, and for each current, $V_{\rm ds} = 6, 8, 10$ V. (c) Magnitude of the correlation coefficient C. (d) Phase of the correlation coefficient C.

V and $I_{\rm ds} = 60$ mA, with the fitted contributions due to velocity fluctuation, $1/f$ noise, and leakage current using

$$\langle |i_g|^2 \rangle = A_1 f^2 + \frac{A_2}{1 + 4\pi^2 f^2 \tau^2} + A_3 \tag{34}$$

$$\langle |i_d|^2 \rangle = B_1 + \frac{B_2}{1 + 4\pi^2 f^2 \tau^2} + B_3 \tag{35}$$

where A_i, B_i, and τ are constant fitting coefficients. The first terms in (34) and (35), with coefficients A_1 and B_1, represent velocity fluctuation noise, and the frequency dependence is suggested by the simplified FET noise model of Fig. 2 [from (2) and (3)]. For Pucel's noise model [28], which accounts for velocity fluctuation (or diffusion) noise only, the coefficients P, R, and C can be extracted from A_1 and B_1 and a linear fit to $\langle i_{g,v} i_{d,v}^* \rangle$, respectively. Thus,

$$\langle |i_{g,v}|^2 \rangle = A_1 f^2 = R 4kT_0 B \left(2\pi f C_{\rm gs}\right)^2 / g_m \tag{36}$$

$$\langle |i_{d,v}|^2 \rangle = B_1 = P 4kT_0 B g_m \tag{37}$$

$$\langle i_{g,v} i_{d,v}^* \rangle = C\sqrt{RP} 4kT_0 B \left(2\pi f C_{\rm gs}\right). \tag{38}$$

For the $1/f$ noise, a single trap speed model is assumed with a time constant τ, and this Lorentzian spectral density has fitting parameters A_2, B_2, and τ [6]. Note that, in this fit, with measurement $f > 1/\tau$, it is not possible to uniquely determine τ. A frequency-independent shot noise model is assumed, and the associated fitting parameters are A_3 and B_3. The coefficient B_3 (drain shot noise) in (35) can be absorbed into B_1 (velocity fluctuation) because both are constants for the frequency range considered; B_3 is also small relative to B_1. The fitting coefficients in (34) and (35) were found using a least mean square error fit, and they are included in Table II for comparison with the measured noise data of the 0.25×250 μm^2 at $V_{\rm ds} = 4$ V and $I_{\rm ds} = 60$ mA.

Fig. 12 shows the results of applying the fits of (34) and (35). As can be seen in Fig. 12(a), the gate noise $\langle |i_g|^2 \rangle$ is primarily influenced by shot (gate leakage current) and $1/f$ noise at lower frequencies, but as the frequency increases, velocity fluctuation noise dominates ($\propto f^2$). The magnitude of the correlated spectral density $|\langle i_g i_d^* \rangle|$ in Fig. 12(b) has an approximately linear dependence with frequency, as the ideal model of (1) suggests, with minimal impact of either shot or $1/f$ noise at lower frequencies ($|\langle i_g i_d^* \rangle| \sim |\langle i_{g,v} i_{d,v}^* \rangle|$). Consistent with the contribution of the independent noise processes, namely, the $1/f$ and gate leakage shot noise in (31) and (32), applied to (30), the extracted $|C|$ decreases with reducing frequency, as shown in Fig. 11(c). In order to deembed the shot noise and account for the frequency dependence of C [magnitude and phase shown in Fig. 11(c) and (d)] correctly, full correlation between $i_{g,\rm shot}$ and $i_{d,\rm shot}$ is assumed, i.e., $\langle i_{g,\rm shot} i_{d,\rm shot}^* \rangle / \sqrt{\langle |i_{g,\rm shot}|^2 \rangle \langle |i_{d,\rm shot}|^2 \rangle} = -1$, with an assumed 180° phase difference between $i_{g,\rm shot}$ and $i_{d,\rm shot}$. For simplicity, zero correlation is assumed for the $1/f$ noise ($\langle i_{g,1/f} i_{d,1/f}^* \rangle = 0$). Fig. 12(c) and (d) shows the extracted C and the result following the removal of shot and $1/f$ noise (C_v)

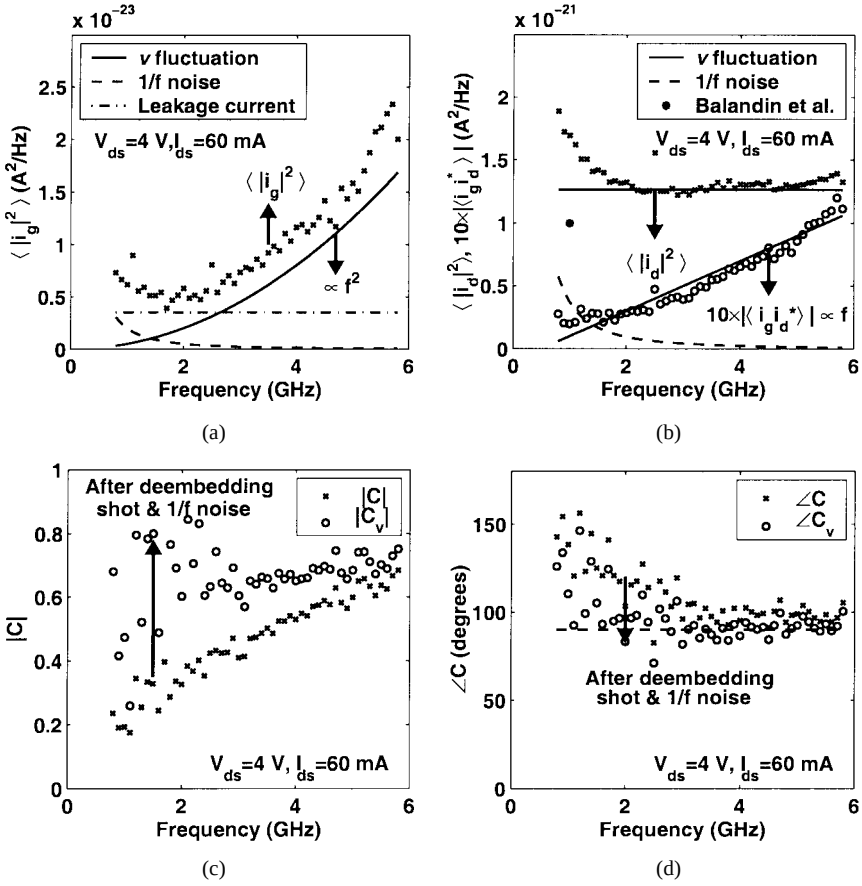

Fig. 12. (a) Extracted $\langle |i_g|^2 \rangle$ with the fitted contributions from velocity fluctuation, leakage current, and $1/f$ noise. The gate noise has a minimum at approximately 2 GHz. (b) Extracted $\langle |i_d|^2 \rangle$ and $|\langle i_g i_d^* \rangle|$. Shown are the shot plus velocity fluctuation and $1/f$ fitting for $\langle |i_d|^2 \rangle$, and the linear fit for $|\langle i_g i_d^* \rangle|$. The point (•) is the extrapolation result from the measured $1/f$ noise current variance for the undoped AlGaN/GaN HEMT from [30]. (c) $|C|$ and the result following removal of shot and $1/f$ noise ($|C_v|$). (d) Phase of C and the result following removal of shot and $1/f$ noise ($\angle C_v$). $V_{\rm ds} = 4$ V and $I_{\rm ds} = 60$ mA.

TABLE II
COEFFICIENTS IN (34) AND (35) TO FIT THE EXTRACTED NOISE SOURCES IN Fig. 12. THE UNIT FOR THESE CONSTANTS IS A^2/Hz, EXCEPT FOR A_1 (A^2/Hz^3) AND τ (ns)

A_1	A_2	A_3	B_1	B_2	B_3	τ
5×10^{-43}	0.76×10^{-22}	0.35×10^{-23}	1.27×10^{-21}	1.43×10^{-20}	0.35×10^{-23}	0.9716

from the total noise. After deembedding the $1/f$ and shot noise, we find that C becomes more nearly frequency independent, as also found in simulations for GaAs devices [29]. Extrapolation of the measured $1/f$ noise in another GaN HEMT [30] [marked with a • in Fig. 12(b)] gives a similar result to our fit. The shot noise determined from the measured gate leakage current ($2eI_{\rm gs} = 0.57 \times 10^{-23}$ A^2/Hz for $V_{\rm ds} = 4$ V and $I_{\rm ds} = 60$ mA, where $I_{\rm gs}$ is the measured gate-to-source dc current) is also close to the fitted result for this noise contribution. Our results are, therefore, consistent with total noise being a superposition of contributions from traps, gate leakage, and channel velocity fluctuation (high-frequency noise).

Fig. 13 shows the extracted magnitude and phase of C (velocity fluctuation only, with the influence of shot and $1/f$ noise deembedded) for the 0.25 × 250 μm^2 and 0.40 × 250 μm^2 AlGaN/GaN HEMTs, showing that the submicrometer (0.25 and 0.4 μm) gate-length GaN HEMT has a correlation coefficient of approximately $j0.7$. The data for $|C|$ in Fig. 13(a) does not show appreciable differences for the two submicrometer gate lengths. A MOSFET noise simulation study has shown an increase in $|C|$ with reducing gate length in the 1–0.25-μm range [31]. The precision of our data is not able to support this trend.

Referring back to Fig. 10(a), the measured $F_{\rm min}$ varies more with $I_{\rm ds}$ at the lower frequencies, and is largest for the smallest $I_{\rm ds}$. This is consistent with gate leakage shot noise, which would be greatest for the most negative $V_{\rm gs}$.

VI. INFLUENCE OF GATE–DRAIN NOISE CORRELATION WITH AN IDEAL MODEL

In order to assess the effect that C has on the total noise, we consider the ideal FET noise model in Fig. 2 (with velocity fluctuation noise only) and calculate $F_{\rm min}$ in terms of $\langle |i_g|^2 \rangle$, $\langle |i_d|^2 \rangle$, and correlation coefficient C, ignoring the noise contribution from parasitics, i.e., setting $\mathbf{C}_d = \mathbf{C}_{pd}$ and $\mathbf{Y}_d = \mathbf{Y}_e$. Using (21) and (30)

$$\mathbf{C}_d = \begin{bmatrix} \langle |i_g|^2 \rangle & j|C|\sqrt{\langle |i_g|^2 \rangle \langle |i_d|^2 \rangle} \\ -j|C|\sqrt{\langle |i_g|^2 \rangle \langle |i_d|^2 \rangle} & \langle |i_d|^2 \rangle \end{bmatrix} \tag{39}$$

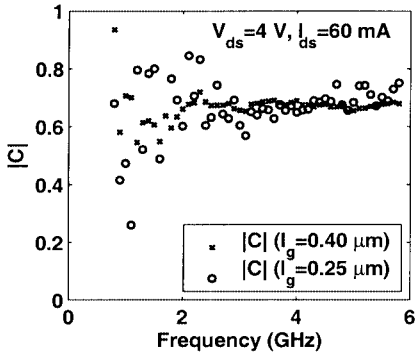

(a)

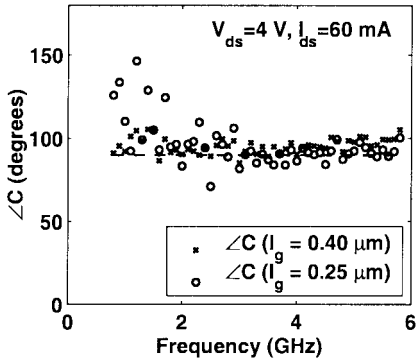

(b)

Fig. 13. Correlation coefficient C due to velocity fluctuation (shot and $1/f$ noise deembedded) for 0.25 × 250 μm^2 and 0.4 × 250 μm^2 AlGaN/GaN HEMTs at $V_{\rm ds} = 4$ V and $I_{\rm ds} = 60$ mA. (a) Magnitude. (b) Phase.

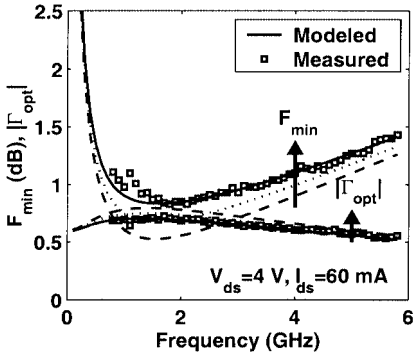

(a)

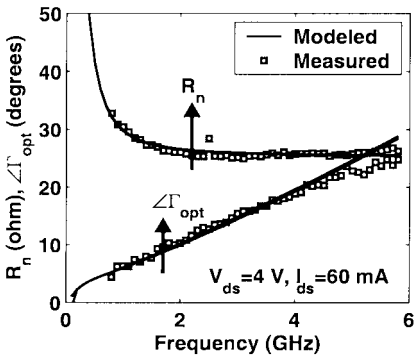

(b)

Fig. 14. (a) Measured and modeled $F_{\rm min}$ and optimum source reflection coefficient $|\Gamma_{\rm opt}|$. (b) Measured and modeled R_n and phase of optimum source reflection coefficient $\Gamma_{\rm opt}$. $V_{\rm ds} = 4$ V and $I_{\rm ds} = 60$ mA. The dotted line is the case with 50% of the estimated leakage and the dashed line is the case with 10% of the leakage current.

$$\mathbf{Y}_d = \begin{bmatrix} j2\pi f C_{\rm gs} & 0 \\ g_m & 0 \end{bmatrix}. \tag{40}$$

$\mathbf{C}_A$ can be obtained by the inverse transformation of (26). Using the relation between the basic noise parameters and $\mathbf{C}_A$ in (13), $F_{\rm min}$ can be expressed as

$$F_{\rm min} = 1 + \frac{2\sqrt{\langle |i_g|^2 \rangle \langle |i_d|^2 \rangle}}{g_m} \sqrt{1 - |C|^2}. \tag{41}$$

Equation (41) indicates that, with no parasitics, perfect correlation ($|C| = 1$) cancels the noise contribution from $\langle |i_{g,v}|^2 \rangle$ and $\langle |i_{d,v}|^2 \rangle$ completely, giving $F_{\rm min} = 1$. Also note that $F_{\rm min}$ in (41) is increasing with frequency because $\langle |i_{g,v}|^2 \rangle$ is directly proportional to f^2; thus, $F_{\rm min} \to 1$ as $f \to 0$. Therefore, high correlation ($j1$ is the theoretical maximum) would be desirable for a low-noise device since correlation is a cancellation term in calculating the total noise of the FET.

VII. Noise Simulation

When gate noise current i_g ($\propto f$) is cast into noise voltage v_g ($= i_g / j2\pi f C_{\rm gs}$) in Fig. 2, we can view the velocity fluctuation noise sources v_g and i_d as being white noise. If the frequency dependence of the $1/f$ noise is known (from, e.g., the single-trap model) and $1/f$ and gate leakage shot noise is deembedded correctly from the total noise ($\mathbf{C}_d$), the resulting noise correlation matrix can be converted into another intrinsic noise matrix $\mathbf{N}$ due to the velocity fluctuation only, resulting in

$$\mathbf{N} = \mathbf{T}^{-1} \mathbf{C}'_d \left(\mathbf{T}^{-1}\right)^H = \begin{bmatrix} \langle v_g v_g^* \rangle & \langle v_g i_d^* \rangle \\ \langle i_d v_g^* \rangle & \langle i_d i_d^* \rangle \end{bmatrix} \tag{42}$$

where $\mathbf{C}'_d$ is the result following the removal of shot and $1/f$ noise, and

$$\mathbf{T} = \begin{bmatrix} \dfrac{j2\pi f C_{\rm gs}}{1 + j2\pi f C_{\rm gs} R_i} & 0 \\ \dfrac{g_m}{1 + j2\pi f C_{\rm gs} R_i} & 1 \end{bmatrix}. \tag{43}$$

Assuming an ideal model with v_g and i_d independent of frequency, all the elements in $\mathbf{N}$ are independent of frequency. Our experimentally extracted results support this contention. Therefore, a single-frequency measurement allows the complete characterization of noise properties due to velocity fluctuation.

In order to validate the noise equivalent-circuit model, the intrinsic noise correlation matrix $\mathbf{N}$, deembedded at 4 GHz, was used to simulate the noise parameters at other frequencies. Using the frequency-independent $\mathbf{N}$, together with the gate leakage current shot noise, plus the $1/f$ noise contribution from a single trap model, $\mathbf{C}_d$ was recalculated at other frequencies. Both the parasitic and intrinsic device equivalent circuits contain reactive components. Thus, the admittance matrices $\mathbf{Y}_d$ and $\mathbf{Y}_p$ are frequency dependent and should also be computed accordingly at other frequencies. Given $\mathbf{C}_p$ [from (28)], $\mathbf{C}_{pd}$ can be calculated using (25), and the new $\mathbf{C}_A$ (i.e., the new noise parameters) at other frequencies are obtained using (13). Fig. 14 shows the simulated noise parameters from the model (solid line) in comparison with the measured data (symbol) for the 0.25 × 250 μm^2 AlGaN/GaN HEMT with $V_{\rm ds} = 4$ V and $I_{\rm ds} = 60$ mA. In Fig. 14, $\Gamma_{\rm opt}$ is the optimum noise reflection

coefficient, expressed as $\Gamma_{\rm opt} = (1 - 50Y_{\rm opt})/(1 + 50Y_{\rm opt})$. The simulated noise parameters using the intrinsic noise sources specified at one frequency show excellent agreement with the measured data. To evaluate the impact of reducing the leakage current, Fig. 14(a) shows the simulated noise parameters with 50% (dotted line) and 10% (dashed line) of the estimated gate leakage current. As indicated in this figure, $F_{\rm min}$ can be minimized by bringing the gate leakage down, while other noise parameters are not affected significantly.

VIII. Conclusion

The emphasis of this study was to determine the precise intrinsic noise sources for AlGaN/GaN HEMTs, thus enabling the development of an accurate noise equivalent-circuit model. Using the measured noise parameters and the deembedding routine presented, the gate and drain noise current sources and their correlation were extracted as a function of bias and frequency. This established a noise equivalent-circuit model that is effective for GaN HEMTs we have fabricated, allowing velocity fluctuation, $1/f$, and gate leakage current shot noise to be incorporated. The model elements determined at one frequency accurately predict the measured frequency-dependent noise characteristics.

Appendix

The expression for the elements of the noise correlation matrix $\mathbf{C}_A$ is derived in terms of the noise parameters $F_{\rm min}$, R_n, and $Y_{\rm opt}$. The $(1,1)$ element of $\mathbf{C}_A$ in (11) is given by (5). Using (4)–(6), the $(2,2)$ element of $\mathbf{C}_A$ is

$$\begin{aligned}\langle |i_A|^2\rangle &= \langle (Y_c v_A + i_u)(Y_c v_A + i_u)^*\rangle \\ &= |Y_c|^2\langle |v_A|^2\rangle + \langle |i_u|^2\rangle \\ &= 4kT_0B\big(|Y_c|^2R_n + G_n\big) \\ &= 4kT_0BR_n\left(\frac{G_n}{R_n} + G_c^2 + B_c^2\right) \end{aligned} \tag{A-1}$$

Applying $G_{\rm opt} = \sqrt{(G_n/R_n) + G_c^2}$ and $B_{\rm opt} = -B_c$ from (8) to (A-1)

$$\langle |i_A|^2\rangle = 4kT_0BR_n\big(G_{\rm opt}^2 + B_{\rm opt}^2\big) = 4kT_0BR_n|Y_{\rm opt}|^2. \tag{A-2}$$

Consider now the off-diagonal terms of $\mathbf{C}_A$. From (8) and (9)

$$F_{\rm min} = 1 + 2R_nG_c + 2R_nG_{\rm opt}. \tag{A-3}$$

Equation (A-3) can be rewritten with R_nG_c and other terms by

$$R_nG_c = \frac{F_{\rm min} - 1}{2} - R_nG_{\rm opt}. \tag{A-4}$$

Using (A-4) and $B_c = -B_{\rm opt}$ from (8)

$$R_nY_c = R_n(G_c + jB_c) = \frac{F_{\rm min} - 1}{2} - R_nY_{\rm opt}. \tag{A-5}$$

Now, the $(1,2)$ element of $\mathbf{C}_A = \langle v_Ai_A^*\rangle$ is

$$\langle v_Ai_A^*\rangle = \langle v_A(Y_c^*v_A^* + i_u^*)\rangle = Y_c^*\langle |v_A|^2\rangle. \tag{A-6}$$

Thus, using (4) and (A-5)

$$\langle v_Ai_A^*\rangle = 4kT_0BR_nY_c^* = 4kT_0B\left(\frac{F_{\rm min} - 1}{2} - R_nY_{\rm opt}^*\right). \tag{A-7}$$

The $(2,1)$ element of $\mathbf{C}_A$ is the complex conjugate of the $(1,2)$ element. Finally, normalizing $\mathbf{C}_A$ (dividing by $4kT_0B$) gives

$$\mathbf{C}_A = \begin{bmatrix} R_n & \dfrac{F_{\rm min} - 1}{2} - R_nY_{\rm opt}^* \\ \dfrac{F_{\rm min} - 1}{2} - R_nY_{\rm opt} & R_n|Y_{\rm opt}|^2 \end{bmatrix}. \tag{A-8}$$

Acknowledgment

The load–pull microwave noise measurement was performed at Motorola Inc., Tempe, AZ. The authors would like to thank Dr. C. E. Weitzel, Digital DNA Laboratories, Motorola Inc., Tempe, AZ, for discussions related to microwave noise measurements.

References

[1] L. F. Eastman, V. Tilak, J. Smart, B. M. Green, E. M. Chumbes, R. Dimitrov, H. Kim, O. S. Ambacher, N. Weimann, T. Prunty, M. Murphy, W. J. Schaff, and J. R. Shealy, "Undoped AlGaN/GaN HEMTs for microwave power amplification," *IEEE Trans. Electron Devices*, vol. 48, pp. 479–485, Mar. 2001.

[2] W. Lu, J. Yang, M. A. Khan, and I. Adesida, "AlGaN/GaN HEMTs on SiC with over 100 GHz f_T and low microwave noise," *IEEE Trans. Electron Devices*, vol. 48, pp. 581–585, Mar. 2001.

[3] T. Hussain, A. Kurdoghlian, P. Hashimoto, W. S. Wong, M. Wetzel, J. S. Moon, L. McCray, and M. Micovic, "GaN HFET's with excellent low noise performance at lower power levels through the use of thin AlGaN Schottky barrier layer," in *Int. Electron Devices Meeting Tech. Dig.*, 2001, pp. 581–584.

[4] W. Y. Ho, C. Surya, K. Y. Tong, W. Kim, A. E. Botcharev, and H. Morkoc, "Characterization of flicker noise GaN-based MODFET's at low drain bias," *IEEE Trans. Electron Devices*, vol. 46, pp. 1099–1104, June 1999.

[5] A. Balandin, S. V. Morozov, S. Cai, R. Li, K. L. Wang, G. Wijeratne, and C. R. Viswanathan, "Low flicker noise GaN/AlGaN heterostructure field effect transistors for microwave communications," *IEEE Trans. Microwave Theory Tech.*, vol. 47, pp. 1413–1417, Aug. 1999.

[6] S. L. Rumyantsev, N. Pala, M. S. Shur, E. Borovitskaya, A. P. Dmitriev, M. E. Levinshtein, R. Gaska, M. A. Khan, J. Yang, X. Hu, and G. Simin, "Generation-recombination noise in GaN/AlGaN heterostructure field effect transistors," *IEEE Trans. Electron Devices*, vol. 48, pp. 530–534, Mar. 2001.

[7] J. Mateos, T. Gonzalez, D. Pardo, V. Hoel, and A. Cappy, "Monte Carlo simulator for the design optimization of low-noise HEMTs," *IEEE Trans. Electron Devices*, vol. 47, pp. 1950–1956, Oct. 2000.

[8] W. Shockley, J. A. Copeland, and R. P. James, "The impedance field method of noise calculation in active semiconductor devices," in *Quantum Theory of Atoms, Molecules, and the Solid State*. New York: Academic, 1966, pp. 537–563.

[9] A. Cappy, "Noise modeling and measurement techniques," *IEEE Trans. Microwave Theory Tech.*, vol. 36, pp. 1–10, Jan. 1988.

[10] H. Rothe and W. Dahlke, "Theory of noisy four poles," *Proc. IRE*, vol. 44, pp. 811–818, June 1956.

[11] H. Fukui, "The noise performance of microwave transistors," *IEEE Trans. Electron Devices*, vol. 13, pp. 329–341, Mar. 1966.

[12] H. Statz, H. A. Haus, and R. A. Pucel, "Noise characteristics of gallium arsenide field-effect transistors," *IEEE Trans. Electron Devices*, vol. ED-21, pp. 549–562, Sept. 1974.

[13] M. W. Pospieszalski, "Modeling of noise parameters of MESFET's and MODFET's and their frequency and temperature dependence," *IEEE Trans. Microwave Theory Tech.*, vol. 36, pp. 1–10, Jan. 1988.

[14] R. A. Pucel, W. Struble, R. Hallgren, and U. L. Rohde, "A general noise de-embedding procedure for packaged two-port linear active devices," *IEEE Trans. Microwave Theory Tech.*, vol. 40, pp. 2013–2024, Nov. 1992.
[15] P. Heymann, M. Rudolph, H. Prinzler, R. Doerner, L. Klapproth, and G. Bock, "Experimental evaluation of microwave field-effect-transistor noise models," *IEEE Trans. Microwave Theory Tech.*, vol. 47, pp. 156–163, Feb. 1999.
[16] J. Stenarson, M. Garcia, I. Angelov, and H. Zirath, "A general parameter-extraction method for transistor noise models," *IEEE Trans. Microwave Theory Tech.*, vol. 47, pp. 2358–2363, Dec. 1999.
[17] S. Lee, V. Tilak, K. J. Webb, and L. F. Eastman, "Intrinsic noise characteristics of AlGaN/GaN HEMTs," in *IEEE MTT-S Int. Microwave Symp. Dig.*, vol. 3, Seattle, WA, June 2002, pp. 1415–1418.
[18] S. Lee, K. J. Webb, V. Tilak, and L. F. Eastman, "Intrinsic AlGaN/GaN HEMT noise from a measurement-based equivalent circuit model," presented at the Device Research Conf. Dig., Santa Barbara, CA, June 2002.
[19] A. van der Ziel, *Noise in Solid State Devices and Circuits*. New York: Wiley, 1986.
[20] H. Nyquist, "Thermal agitation of electric charge in conductors," *Phys. Rev.*, vol. 32, pp. 110–113, July 1928.
[21] M. Mitama and H. Katoh, "An improved computational method for noise parameter measurement," *IEEE Trans. Microwave Theory Tech.*, vol. MTT-27, pp. 612–615, June 1979.
[22] C. H. Chen, M. J. Deen, Y. Cheng, and M. Matloubian, "Intrinsic noise currents in deep submicron MOSFETs," in *IEEE MTT-S Int. Microwave Symp. Dig.*, vol. 2, Phoenix, AZ, May 2001, pp. 835–839.
[23] H. Hillbrand and P. H. Russer, "An efficient method for computer aided noise analysis of linear amplifier networks," *IEEE Trans. Circuits Syst.*, vol. 23, pp. 235–238, Apr. 1976.
[24] R. Q. Twiss, "Nyquist's and Thevenin's theorems generalized for nonreciprocal linear networks," *J. Appl. Phys.*, vol. 26, no. 5, pp. 599–602, May 1955.
[25] B. M. Green, K. K. Chu, E. M. Chumbes, J. A. Smart, J. R. Shealy, and L. F. Eastman, "The effect of surface passivation on the microwave characteristics of undoped AlGaN/GaN HEMT's," *IEEE Electron Device Lett.*, vol. 21, pp. 268–270, June 2000.
[26] "Noise parameter measurement using the HP 8970B noise figure meter and the ATN NP4 noise parameter test set," Agilent Technol., Product note HP 8970B/S-3.
[27] B. M. Green, "Characteristics, integration and optimization of integrated circuits on AlGaN/GaN HEMTs," Ph.D. dissertation, School Elect. Comput. Eng., Cornell Univ., Ithaca, NY, 2001.
[28] R. A. Pucel, H. A. Haus, and H. Statz, *Advances in Electronics and Electron Physics*. New York: Academic, 1975, vol. 38.
[29] F. Dannevill, G. Dambrine, H. Happy, P. Tadyszak, and A. Cappy, "Influence of the gate leakage current on the noise performance of MESFET's and MODFETs," *Solid State Electron.*, vol. 38, no. 5, pp. 1081–1087, May 1995.
[30] A. Balandin and K. L. Wang, "Noise spectroscopy of traps in GaN devices," in *IEEE Int. Compound Semiconductors Symp. Dig.*, Monterey, CA, Oct. 2000, pp. 501–506.
[31] J. S. Goo, C. H. Choi, F. Danneville, E. Morifuji, H. S. Momose, Z. Yu, H. Iwai, T. H. Lee, and R. W. Dutton, "An accurate and efficient high frequency noise simulation technique for deep submicron MOSFETs," *IEEE Trans. Electron Devices*, vol. 47, pp. 2410–2419, Dec. 2000.

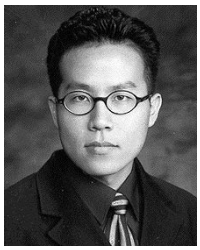

Sungjae Lee (S'98) received the B.S. degree in electrical engineering from the Seoul National University, Seoul, Korea, in 1998, the M.S. degree from Purdue University, West Lafayette, IN, in 2000, and is currently working toward the Ph.D. degree at Purdue University.

His current research interests encompass broad-band power-amplifier design and noise characterization and modeling of AlGaN/GaN HEMTs. During the summer of 2001, he was an Intern with the Digital DNA Laboratories, Motorola Inc., Tempe, AZ.

Mr. Lee is a member of Eta Kappa Nu.

Kevin J. Webb (S'81–M'84–SM'98) received the B.Eng. and M.Eng. degrees from the Royal Melbourne Institute of Technology, Melbourne, Australia, in 1978 and 1983, respectively, the M.S.E.E. degree from the University of California at Santa Barbara, in 1981, and the Ph.D. degree from the University of Illinois at Urbana-Champaign, in 1984.

He is currently a Professor with the School of Electrical and Computer Engineering, Purdue University.

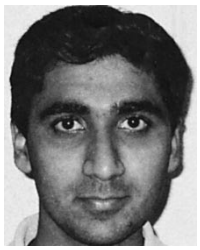

Vinayak Tilak was born in Chennai, India. He received the M.Sc. degree in physics and B.E. degree in electrical engineering from the Birla Institute of Technology and Science, Pilani, India, in 1997, and the Ph.D. degree in applied and engineering physics from Cornell University, Ithaca, NY, in 2002.

He is currently with Central Research and Development Laboratories, General Electric, Niskayuna, NY. His research interests include high-power microwave transistors, gallium transistor technology, and device physics.

Lester F. Eastman (A'53–M'58–SM'65–F'69–LF'94) is currently the John L. Given Foundation Chair Professor of Engineering at Cornell University, Ithaca, NY. Beginning in 1998, he became devoted full time to graduate research and currently has nine graduate students under his supervision. In 1957, he joined the faculty of electrical engineering at Cornell University. He also serves as a member of the graduate fields of applied physics and materials science. Since 1965, he has conducted research on compound semiconductor materials and high-speed devices and circuits, and has been active in organizing workshops and conferences on these subjects elsewhere since 1965 and at Cornell University since 1967. In 1977, he joined other Cornell University faculty members in obtaining funding and founding the National Research and Resource Facility for Submicron Structures at Cornell (now Cornell Nanofabrication Facility). Also in 1977, he founded the Joint Services Electronics Program and directed it until 1987. He has supervised over 100 Ph.D. dissertations, over 50 M.S. theses, and over 50 post-doctoral studies. In his research group, effort is underway on molecular beam epitaxy, microwave transistors, high-speed semiconductor lasers, and fundamental phenomena in compound semiconductor quantum electron and optical devices. From 1978 to 1979, he was on leave at the Massachusetts Institute of Technology (MIT) Lincoln Laboratory, and from 1985 to 1986, he was with the IBM Watson Research Laboratory. He has served as a consultant for several industries.

Dr. Eastman is a member of the National Academy of Engineering (since 1986) and was appointed the John L. Given Foundation Chair Professor of Engineering at Cornell University in January 1985. In 2001, he became a Fellow of the American Physical Society. During 1983, he was the IEEE Electron Device Society National Lecturer. He was a member of the U.S. Government Advisory Group on Electron Devices from 1978 to 1988. From 1987 to 1993, he served as a member of the Kuratorium (Visiting Senior Advisory Board) of the Fraunhofer Applied Physics Institute, Freiburg, Germany. He was the recipient of the 1991 GaAs Symposium Award and the Heinrich Welker Medal for his "contributions to the development of ballistic electron devices, planar doping, buffer layers, and Al1nAs/GaInAs/InP heterostructures." He was also the recipient of the 1994 Alexander von Humboldt Senior Fellowship and the 1995 Aldert van der Ziel Award. He was the recipient of the 1999 IEEE Graduate Teaching Award, the 2000 IEEE Third Millennium Medal, and the 2002 J. J. Ebers Award of the IEEE Electron Device Society.